PROCEEDINGS OF SCIENCE

Seasonal Variations of the Atmospheric Neutrino Flux measured in IceCube

The IceCube Collaboration
(a complete list of authors can be found at the end of the proceedings)

E-mail: karolin.hymon@tu-dortmund.de

The IceCube Neutrino Observatory measures high energy atmospheric neutrinos with high statistics. These atmospheric neutrinos are produced in cosmic ray interactions in the atmosphere, mainly by the decay of pions and kaons. The rate of the measured neutrinos is affected by seasonal temperature variations in the stratosphere, which are expected to increase with the energy of the particle. In this contribution, seasonal energy spectra are obtained using a novel spectrum unfolding approach, the *Dortmund Spectrum Estimation Algorithm* (DSEA+), in which the energy distribution from 125 GeV to 10 TeV is estimated from measured quantities with machine learning algorithms. The seasonal spectral difference to the annual average flux will be discussed based on preliminary results from IceCube's atmospheric muon neutrino data.

Corresponding authors: Karolin Hymon[1*], Tim Ruhe[1]
[1] *Astroparticle Physics WG Rhode, TU Dortmund University, Germany*
[*] Presenter

The 38th International Cosmic Ray Conference (ICRC2023)
26 July – 3 August, 2023
Nagoya, Japan

© Copyright owned by the author(s) under the terms of the Creative Commons Attribution-NonCommercial-NoDerivatives 4.0 International License (CC BY-NC-ND 4.0).

PoS(ICRC2023)993

1. Introduction

For current neutrino telescopes, lepton fluxes originating from cosmic ray interactions in the atmosphere impose a challenging background in identifying scarce astrophysical neutrinos. Besides the requirement of an accurate understanding of leptonic fluxes for detector calibration, they serve as indicators of probing hadronic interactions within cosmic ray-induced particle showers in the atmosphere.

A hadronic cascade of mesons, mainly composed of kaons and pions, is initiated by an interaction of a primary cosmic ray in the upper atmosphere [1]. Conventional atmospheric muons and neutrinos are produced in weak decays by these parent mesons. The relative probability for their decay or re-interaction inside the atmosphere is at equilibrium at the critical energy for each individual meson. The critical energy at a given atmospheric depth is proportional to the local atmospheric air density, which changes anti-proportionally with temperature. The probability of decay increases with temperature so that the muon and neutrino flux becomes temperature-dependent. The flux modulation based on temperature evaluation throughout the year is referred to as seasonal variations. A more detailed overview on the formalism can be found in [1, 2].

The modulation of the seasonal muon and neutrino rate has been studied extensively with respect to atmospheric temperature in various experiments, e. g. [2–5], but no energy-dependent measurement of the spectral shape has been conducted on a seasonal basis. In this contribution, we present an update on the progenitor analysis from [6] to 11.5 years of neutrino data from IceCube providing a measurement of the seasonal muon neutrino flux variations with respect to energy.

2. Neutrino Data

The IceCube Neutrino Observatory is a neutrino detector in the Antarctic ice at the geographic South Pole, located between depths of 1450 m and 2450 m with a comprised instrumented volume of a cubic kilometer. The detector array consists of 86 vertical cable strings which are equipped with 5160 digital optical modules (DOMs) in total. Energy, flavor, and directional reconstruction of the neutrinos rely on the optical detection of initiated Cherenkov radiation by charged particles produced in the interactions of neutrinos in the surrounding ice or the nearby bedrock [7].

The data sample consists of well reconstructed up-going tracks, classified as muons induced by neutrino interactions inside the ice, with a purity of more than 99.7% [8]. Down-going neutrinos, produced in cosmic ray induced air showers vertically above Antarctica, are excluded in this analysis as these events are hardly distinguishable within the dominating background of atmospheric muons from the same showers. The zenith arrival direction, θ, of the neutrinos is restricted to the Southern Hemisphere within 90° to 120° below the Tropic of Capricorn. Seasonal temperature variations at production heights of the neutrinos are required for this analysis. The Northern Hemisphere is excluded. A deeper description of the zenith direction and temperature variation throughout the year is given in [5]. The analysis includes events from May 2011 to December 2022, in which the full detector configuration was complete. This results in 523736 neutrino events within 11.3 years of effective livetime.

PoS(ICRC2023)993

3. Spectrum Unfolding

The determination of the neutrino energy is an inverse problem as it needs to be inferred from an energy proxy of the induced muon in the ice. The muon, however, is exposed to stochastic energy losses and ionization, which in turn smears out the energy resolution. This inverse problem is addressed by a spectrum unfolding technique with an incorporated machine learning algorithm. The *Dortmund Spectrum Estimation Algorithm* (DSEA+) [9] estimates the probability of a given event corresponding to one of the predefined energy bins in terms of a multinomial classification task, which is performed in an iterative manner. The energy is estimated from two proxies, the number of DOMs triggered in each event and an energy reconstruction for the induced muon track [10]. For further explanation of DSEA+ and the optimized internal parameters refer to [6]. In contrast to the previous work described in [6], the unfolding algorithm is trained on Monte Carlo simulation weighted to the neutrino flux calculated by MCEq [11]. MCEq solves the cascade equations of particle interactions in atmospheric cosmic ray air showers numerically, based on different theoretical models. The H3a model [12] is selected as primary composition model of the cosmic rays, SIBYLL2.3c [13] as hadronic interaction model, and NRLMSISE-00 [14] as the empirical atmospheric model. DSEA+ is trained on the annual average predicted flux. No seasonal information is fed into the algorithm so that the seasonal variations strength can be determined independently of prior assumptions on the expected variation strength. The algorithm is robust against changes in spectral shape compared to its training spectrum so that an observation of deviations in spectral shape caused by seasonal variations is feasible.

The effect of systematic uncertainties on the unfolded spectrum is estimated from simulations with varied detector settings. Pseudo-samples are unfolded and the deviation to the reference unfolded pseudo-sample of average systematic parameters is evaluated for upper and lower constraints on each effect, elaborated below. All associated uncertainties are combined in the quadratic sum for each of the individual positive and negative deviations from the reference unfolded spectrum [6]. The efficiency of the optical modules in IceCube, the absorption and scattering effects in the glacial ice, and the optical properties of the re-frozen ice of the borehole around the strings are estimated from Monte Carlo simulation with varied respective parameter. The uncertainty of the imposed neutrino flux from MCEq in the weighting of the training sample can be constrained by the propagation of uncertainties from the primary cosmic ray composition and hadronic interaction models, as described in [15]. The propagated uncertainties of the neutrino flux are linearly interpolated between 100 GeV and 10 TeV. Two additional pseudo-samples are weighted to the upper and lower limit of the neutrino flux uncertainty and unfolded. The statistical uncertainty is determined by bootstrapping [16], in which the events from the seasonal data sets are sampled with replacement in 2000 trials and the standard deviation is calculated for the unfolded number of events in each energy bin. To convert the unfolded event spectrum into a differential flux, the effective area needs to be obtained from Monte Carlo simulations of the detector response and the spectrum is accounted for livetime of the seasonal data sets and solid angle of the arrival directions.

PoS(ICRC2023)993

4. Results

The seasonal spectra are unfolded in ten equidistant bins in $\log(E_\nu)$ from 125 GeV to 10 TeV and the variation strength is determined with respect to the annual average neutrino flux. The seasonal flux ratio is merely affected by propagation of the statistical uncertainties of the unfolded rates because the systematic uncertainties are largely independent of the season. Fig. 1 displays the unfolded seasonal fluxes for two different zenith regions, explained below. The upper panel in each figure shows the unfolded seasonal spectra scaled to E^3. The corresponding systematic uncertainties are shown in the shaded bands. The calculated fluxes from MCEq (with H3a, SIBYLL2.3c, NRLMSISE-00) are shown for comparison and are scaled up to match the normalization of the unfolded spectra. The scaling factor is determined by a fit to the unfolded spectrum with respect to the systematic and statistical uncertainties. The loss function considering the asymmetric error bars of the unfolded spectrum is minimized by the Nelder-Mead [17] approach and a scaling factor of 1.25 is obtained as best-fit value. The lower panel in each figure displays the ratio of the seasonal fluxes to the annual average flux. The ratio displays only statistical uncertainties because the systematic uncertainties cancel out in the ratio as described above. This allows to observe the increase in variation strength with increasing energy at per cent level.

Fig. 1(a) depicts the unfolded spectra for austral summer (December to February) and winter (June to August) within zenith angles from 90° to 120°. The unfolded fluxes are in agreement in shape with the seasonal MCEq fluxes. The energy spectrum is flat in the first energy bin due to threshold effects and declines with increasing energy. The observed seasonal variations increase with the neutrino energy up to 4 TeV, as predicted by MCEq. The increase in seasonal variation strength with increasing particle energy is attributed to the interactions of the secondary mesons in the upper stratosphere. High-energy primary cosmic rays interact higher in the atmosphere and produce secondaries at higher altitude, where the temperature variation throughout the year is larger. However, the observed variations decrease above 4 TeV, which is not consistent with the MCEq prediction.

To investigate the seasonal variation measurement and the observed decline at energies above 4 TeV in detail, the monthly average neutrino rate is investigated in zenith bands of $\Delta\theta = 10°$ width. The three upper panels in Fig. 2 depict the relative average monthly neutrino rate variation with respect to the annual average in the respective zenith bands. The statistical uncertainty is depicted as error bars. The predicted variations from MCEq (H3a, SIBYLL2.3c) are shown in dashed lines based on the assumption of two different atmospheres. Besides the prediction using the atmospheric model NRLMSISE-00, as for the algorithm training and comparison to the unfolded spectra, a data-based prediction is obtained from temperature data from the Atmospheric Infrared Sounder (AIRS) [18] on NASA's Aqua satellite. The satellite orbits the Earth twice per day and the AIRS instrument provides a temperature measurement at pressure levels from 0.1 hPa to 1000 hPa with an angular resolution of $1° \times 1°$ per longitude and latitude. The predicted neutrino rate from MCEq is calculated with daily temperature data from April 2012 - April 2017, as in [2], and the obtained daily rate is averaged per month. The first upper panel in Fig. 2 shows the rate variation between zenith angles from 90° to 100°. The maximum seasonal variation strength of $(4 \pm 2)\%$ is observable in December and January, the minimum of $(6 \pm 2)\%$ in July. The variation strength linearly decreases from January to July, a steep increase is observable from July to October. The

PoS(ICRC2023)993

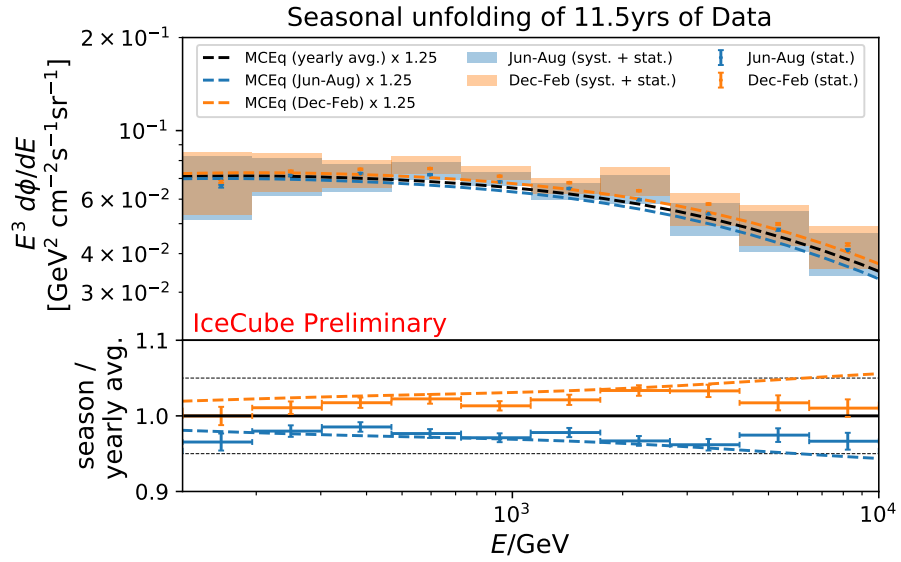

(a) Zenith range: 90° to 120°

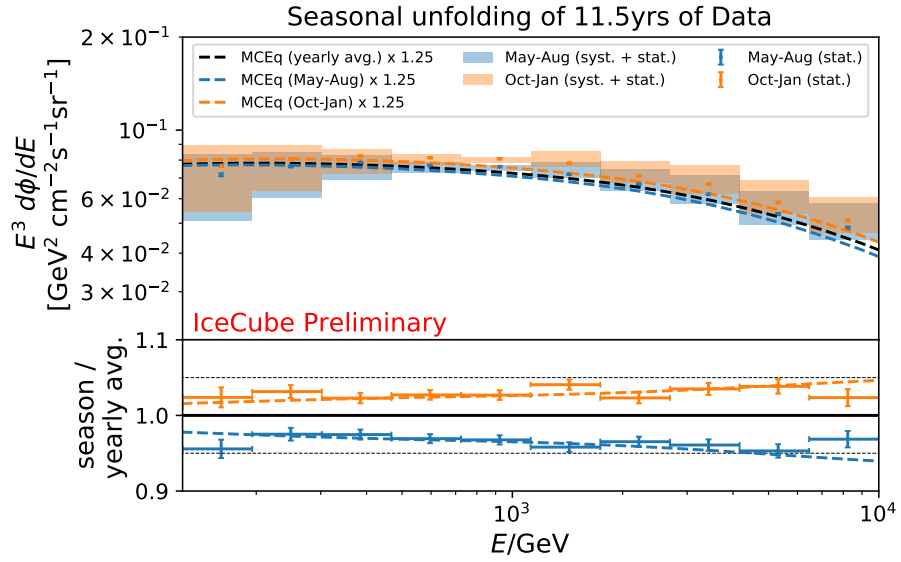

(b) Zenith range: 90° to 110°

Figure 1: Upper panel: unfolded seasonal muon neutrino spectra for austral summer and winter obtained from 11.5 years of IceCube data in the zenith range from 90° to 120° (a) and from 90° to 110° (b). Error bars denote statistical uncertainties, the bands the corresponding systematic uncertainty. The respective predicted flux from MCEq is shown in dashed lines with fitted normalization. Lower panel: ratio of the seasonal to annual average flux for both, the unfolded data and MCEq predictions. Flux deviations of ±5% are marked as black dashed lines. Systematic uncertainties remain the same for each season and cancel out in the ratio.

PoS(ICRC2023)993

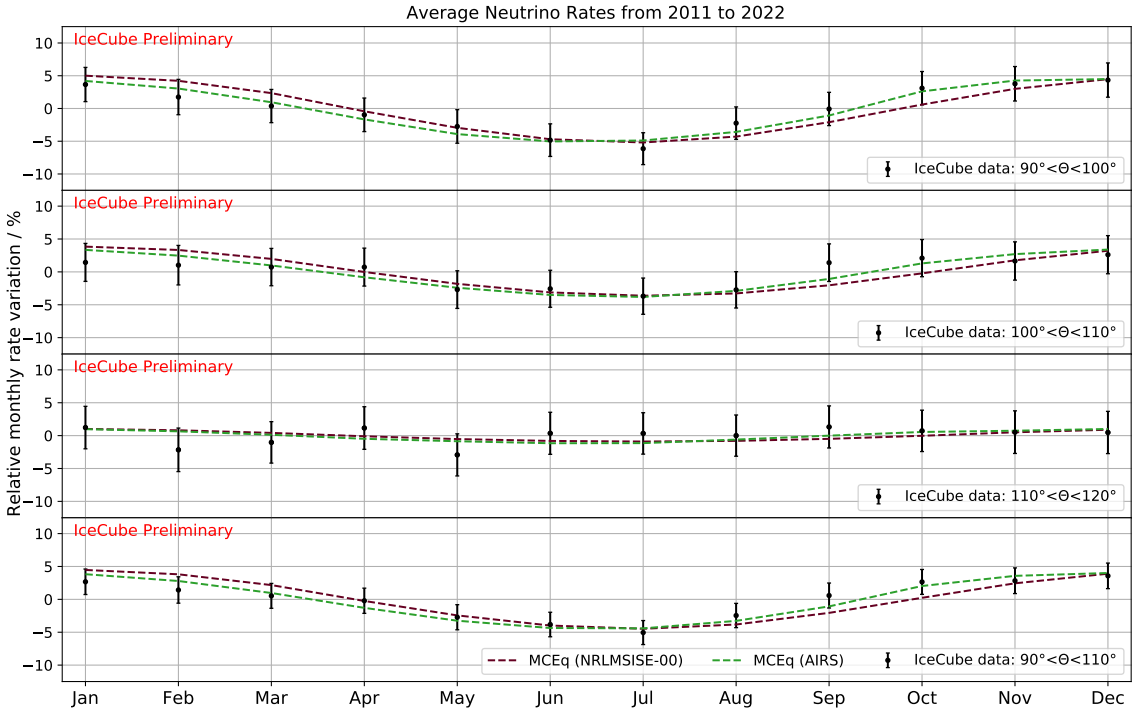

Figure 2: Relative average neutrino rate modulation per month compared to yearly average for the zenith ranges between 90° to 100°, 100° to 110°, 110° to 120° and 90° to 110° including statistical uncertainties. Predicted variations from MCEq are depicted in dashed lines for the atmospheric model NRLMSISE-00 and for five available years of temperature data from the AIRS instrument.

predicted variations from MCEq are both compatible with the observed neutrino rate within the statistical uncertainties. The predicted variation strength amplitude using AIRS data is approx. 1% to 2% higher compared to the calculated prediction with the atmospheric model NRLMSISE-00, except for June and July. The second panel depicts the relative rate variation between 100° to 110°. The variation strength decreases over all months compared to the previous zenith range. The rate variation reaches its maximum of approx. $(2.5 \pm 2.5)\%$ in December, the minimum with $(4 \pm 2.5)\%$ in July. The variation remains roughly constant from January to April and decreases from May to August. The third panel displays the zenith region from 110° to 120°. No variation is evident in the observed neutrino rate. The predicted variations are comparable for both atmospheric assumptions and fluctuate around 0%.

Since no seasonal variations are observed within the third zenith band, a deeper investigation of the seasonal modulation is conducted by removing events arriving from zenith angles between 110° to 120°. The zenith range from 90° to 110° is depicted in the lower panel in Fig. 2. The maximum relative rate variation is in December with $(4 \pm 2)\%$, the minimum in July with $(5 \pm 2)\%$. The variation strength decreases smoothly and slowly from January to July, which is attributed to radiation cooling in the atmosphere, whereas a steep increase in the rate from July to October is likely originating from rapid warming of the stratosphere during sunrise in the Southern Hemisphere. A similar modulation pattern is observed in the muon rate measured in IceCube and its progenitor detector AMANDA [4]. The observed rate variation is similar to the rate variation in the zenith

PoS(ICRC2023)993

range between 90° to 100° in the upper panel in Fig. 2. It indicates that the seasonal modulation within 90° to 110° is dominated by events close to the horizon. The zenith distribution of the neutrino sample is shown in 3. The zenith cut at $\Theta = 110°$ results in a reduction of 26% of neutrino events in the same detector uptime.

Fig. 1(b) displays the seasonal unfolding for the zenith range from 90° to 110°.The definition of austral summer (October to January) and winter (May to August) are adjusted compared to Fig. 1(a) by the selection of months with similar average monthly neutrino rates, observable in Fig. 2. The unfolded seasonal event samples of both zenith bands have comparable statistics so that the reduction of the zenith region does not impact the measurement sensitivity. The unfolded energy spectra are comparable to the spectra in Fig. 1(a) with the same fitted scaling factor for the MCEq normalization. The ratio of the unfolded seasonal flux to the annual average increases with energy from approx. (2 ± 1)% at 125 GeV up to (4 ± 1)% at 7 TeV for October to January. Despite a drop in the ratio to approx. (4.5 ± 1)% in the first energy bin, the ratio decreases up to 7 TeV for May to August, as expected from MCEq. A decrease in the seasonal variation strength with an absolute value of approx. 2.5% is apparent in the highest energy bin between 7 TeV to 10 TeV for both austral summer and winter.

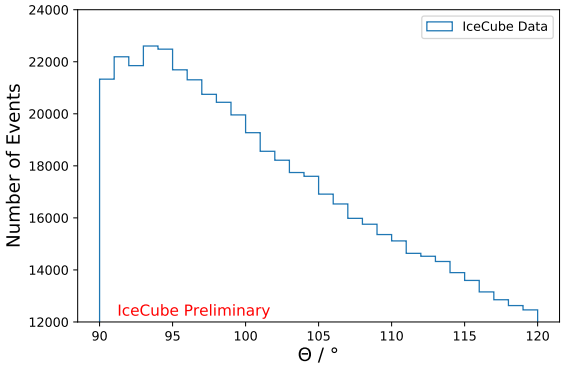

Figure 3: Zenith distribution of the neutrino sample.

5. Conclusion

This work presents the first measurement of seasonal atmospheric muon neutrinos spectra in the zenith range from 90° to 120° and 90° to 110°. The zenith region from 110° to 120° is removed for further investigation as no seasonal modulation is observable. The unfolded modulation of the austral summer and winter relative flux variation for neutrinos from the zenith region between 90° to 110° increases with the neutrino energy up to 7 TeV. The observed pattern is expected, as the interactions of the parent meson becomes the dominant process with increasing energy compared to instant decay. These interactions occur at higher altitudes in the stratosphere, which have a stronger relative temperature modulation throughout the year than lower altitudes. However, the observed variation strength decreases between 7 TeV to 10 TeV despite the expectation from MCEq. Further investigations are required to determine the cause of the decline. The prompt component of the atmospheric neutrino flux, defined as neutrinos produced by prompt decays from charmed mesons, has not been observed so far. This component is seasonally-independent due to the instant decay of the parent particle. However, this component is expected to have a dominant contribution to the atmospheric neutrino flux only above 100 TeV [1], so it is unlikely that the decrease in variation strength at few TeV is attributed to prompt neutrinos. Furthermore, the seasonal modulation at high energies can be investigated by analyzing sub-samples defining a finer seasonal grid throughout the year. The detector enhancement to IceCube-Gen2 [19] and the collection of additional data will constrain the measurement of seasonal variations even further while reducing the statistical

PoS(ICRC2023)993

uncertainty. An extension of the energy range beyond 10 TeV would give conclusion whether the trend of decreasing seasonal variation strength persists due the increasing contribution of prompt neutrinos to the conventional atmospheric flux.

References

[1] T. K. Gaisser, R. Engel, and E. Resconi, *Cosmic Rays and Particle Physics*. Cambridge University Press, 2 ed., 2016.

[2] **IceCube** Collaboration, R. Abbasi *et al.* arXiv:2303.04682.

[3] **MACRO** Collaboration, M. Ambrosio *et al.* *Astropart. Phys.* **7** (1997) 109–124.

[4] **IceCube** Collaboration *PoS* **ICRC2009** (2010) 10.

[5] **IceCube** Collaboration *PoS* **ICRC2019** (2020) 465.

[6] **IceCube** Collaboration *PoS* **ICRC2021** (2021) 1159.

[7] **IceCube** Collaboration, M. G. Aartsen *et al.* *JINST* **12** no. 03, (2017) P03012.

[8] **IceCube** Collaboration, M. G. Aartsen *et al.* *ApJ* **833** (2016) 3.

[9] M. Bunse *https://sfb876.tu-dortmund.de/deconvolution/index.html* .

[10] **IceCube** Collaboration, R. Abbasi *et al.* *Nucl. Instrum. Meth. A* **703** (2013) 190–198.

[11] A. Fedynitch, R. Engel, T. K. Gaisser, F. Riehn, and T. Stanev *EPJ Web Conf.* **99** (2015) 08001.

[12] T. K. Gaisser *Astroparticle Physics* **35** (2011) 801–806.

[13] F. Riehn, R. Engel, A. Fedynitch, T. K. Gaisser, and T. Stanev *PoS* **ICRC2015** (2016) 558.

[14] J. Picone, A. Hedin, D. Drob, and A. Aikin *Journal of Geophysical Research* **107** (12, 2002) .

[15] A. Fedynitch, J. Becker Tjus, and P. Desiati *Phys. Rev. D* **86** (Dec, 2012) 114024.

[16] B. Efron and R. Tibshirani *Statistical Science* **1** (1986) 54–75.

[17] J. A. Nelder and R. Mead *Computer Journal* **7** (1965) 308–313.

[18] I. S. T. Teixeira, "IRS/Aqua L3 Daily Standard Physical Retrieval (AIRS-only) 1 degree x 1 degree V006, Greenbelt, MD, USA, Goddard Earth Sciences Data and Information Services Center (GES DISC)." `https://acdisc.gesdisc.eosdis.nasa.gov/data/Aqua_AIRS_Level3/AIRS3STD.006`.

[19] **IceCube** Collaboration, M. G. Aartsen *et al.* *Journal of Physics G: Nuclear and Particle Physics* **48** (06, 2021) 060501.

PoS(ICRC2023)993

Full Author List: IceCube Collaboration

R. Abbasi[17], M. Ackermann[63], J. Adams[18], S. K. Agarwalla[40, 64], J. A. Aguilar[12], M. Ahlers[22], J.M. Alameddine[23], N. M. Amin[44], K. Andeen[42], G. Anton[26], C. Argüelles[14], Y. Ashida[53], S. Athanasiadou[63], S. N. Axani[44], X. Bai[50], A. Balagopal V.[40], M. Baricevic[40], S. W. Barwick[30], V. Basu[40], R. Bay[8], J. J. Beatty[20, 21], J. Becker Tjus[11, 65], J. Beise[61], C. Bellenghi[27], C. Benning[1], S. BenZvi[52], D. Berley[19], E. Bernardini[48], D. Z. Besson[36], E. Blaufuss[19], S. Blot[63], F. Bontempo[31], J. Y. Book[14], C. Boscolo Meneguolo[48], S. Böser[41], O. Botner[61], J. Böttcher[1], E. Bourbeau[22], J. Braun[40], B. Brinson[6], J. Brostean-Kaiser[63], R. T. Burley[2], R. S. Busse[43], D. Butterfield[40], M. A. Campana[49], K. Carloni[14], E. G. Carnie-Bronca[2], S. Chattopadhyay[40, 64], N. Chau[12], C. Chen[6], Z. Chen[55], D. Chirkin[40], S. Choi[56], B. A. Clark[19], L. Classen[43], A. Coleman[61], G. H. Collin[15], A. Connolly[20, 21], J. M. Conrad[15], P. Coppin[13], P. Correa[13], D. F. Cowen[59, 60], P. Dave[6], C. De Clercq[13], J. J. DeLaunay[58], D. Delgado[14], S. Deng[1], K. Deoskar[54], A. Desai[40], P. Desiati[40], K. D. de Vries[13], G. de Wasseige[37], T. DeYoung[24], A. Diaz[15], J. C. Díaz-Vélez[40], M. Dittmer[43], A. Domi[26], H. Dujmovic[40], M. A. DuVernois[40], T. Ehrhardt[41], P. Eller[27], E. Ellinger[62], S. El Mentawi[1], D. Elsässer[23], R. Engel[31, 32], H. Erpenbeck[40], J. Evans[19], P. A. Evenson[44], K. L. Fan[19], K. Fang[40], K. Farrag[16], A. R. Fazely[7], A. Fedynitch[57], N. Feigl[10], S. Fiedlschuster[26], C. Finley[54], L. Fischer[63], D. Fox[59], A. Franckowiak[11], A. Fritz[41], P. Fürst[1], J. Gallagher[39], E. Ganster[1], A. Garcia[14], L. Gerhardt[9], A. Ghadimi[58], C. Glaser[61], T. Glauch[27], T. Glüsenkamp[26, 61], N. Goehlke[32], J. G. Gonzalez[44], S. Goswami[58], D. Grant[24], S. J. Gray[19], O. Gries[1], S. Griffin[40], S. Griswold[52], K. M. Groth[22], C. Günther[1], P. Gutjahr[23], C. Haack[26], A. Hallgren[61], R. Halliday[24], L. Halve[1], F. Halzen[40], H. Hamdaoui[55], M. Ha Minh[27], K. Hanson[40], J. Hardin[15], A. A. Harnisch[24], P. Hatch[33], A. Haungs[31], K. Helbing[62], J. Hellrung[11], F. Henningsen[27], L. Heuermann[1], N. Heyer[61], S. Hickford[62], A. Hidvegi[54], C. Hill[16], G. C. Hill[2], K. D. Hoffman[19], S. Hori[40], K. Hoshina[40, 66], W. Hou[31], T. Huber[31], K. Hultqvist[54], M. Hünnefeld[23], R. Hussain[40], K. Hymon[23], S. In[56], A. Ishihara[16], M. Jacquart[40], O. Janik[1], M. Jansson[54], G. S. Japaridze[5], M. Jeong[56], M. Jin[14], B. J. P. Jones[4], D. Kang[31], W. Kang[56], X. Kang[49], A. Kappes[43], D. Kappesser[41], L. Kardum[23], T. Karg[63], M. Karl[27], A. Karle[40], U. Katz[26], M. Kauer[40], J. L. Kelley[40], A. Khatee Zathul[40], A. Kheirandish[34, 35], J. Kiryluk[55], S. R. Klein[8, 9], A. Kochocki[24], R. Koirala[44], H. Kolanoski[10], T. Kontrimas[27], L. Köpke[41], C. Kopper[26], D. J. Koskinen[22], P. Koundal[31], M. Kovacevich[49], M. Kowalski[10, 63], T. Kozynets[22], J. Krishnamoorthi[40, 64], K. Kruiswijk[37], E. Krupczak[24], A. Kumar[63], E. Kun[11], N. Kurahashi[49], N. Lad[63], C. Lagunas Gualda[63], M. Lamoureux[37], M. J. Larson[19], S. Latseva[1], F. Lauber[62], J. P. Lazar[14, 40], J. W. Lee[56], K. Leonard DeHolton[60], A. Leszczyńska[44], M. Lincetto[11], Q. R. Liu[40], M. Liubarska[25], E. Lohfink[41], C. Love[49], C. J. Lozano Mariscal[43], L. Lu[40], F. Lucarelli[28], W. Luszczak[20, 21], Y. Lyu[8, 9], J. Madsen[40], K. B. M. Mahn[24], Y. Makino[40], E. Manao[27], S. Mancina[40, 48], W. Marie Sainte[40], I. C. Mariş[12], S. Marka[46], Z. Marka[46], M. Marsee[58], I. Martinez-Soler[14], R. Maruyama[45], F. Mayhew[24], T. McElroy[25], F. McNally[38], J. V. Mead[22], K. Meagher[40], S. Mechbal[63], A. Medina[21], M. Meier[16], Y. Merckx[13], L. Merten[11], J. Micallef[24], J. Mitchell[7], T. Montaruli[28], R. W. Moore[25], Y. Morii[16], R. Morse[40], M. Moulai[40], T. Mukherjee[31], R. Naab[63], R. Nagai[16], M. Nakos[40], U. Naumann[62], J. Necker[63], A. Negi[4], M. Neumann[43], H. Niederhausen[24], M. U. Nisa[24], A. Noell[1], A. Novikov[44], S. C. Nowicki[24], A. Obertacke Pollmann[16], V. O'Dell[40], M. Oehler[31], B. Oeyen[29], A. Olivas[19], R. Ørsøe[27], J. Osborn[40], E. O'Sullivan[61], H. Pandya[44], N. Park[33], G. K. Parker[4], E. N. Paudel[44], L. Paul[42, 50], C. Pérez de los Heros[61], J. Peterson[40], S. Philippen[1], A. Pizzuto[40], M. Plum[50], A. Pontén[61], Y. Popovych[41], M. Prado Rodriguez[40], B. Pries[24], R. Procter-Murphy[19], G. T. Przybylski[9], C. Raab[37], J. Rack-Helleis[41], K. Rawlins[3], Z. Rechav[40], A. Rehman[44], P. Reichherzer[11], G. Renzi[12], E. Resconi[27], S. Reusch[63], W. Rhode[23], B. Riedel[40], A. Rifaie[1], E. J. Roberts[2], S. Robertson[8, 9], S. Rodan[56], G. Roellinghoff[56], M. Rongen[26], C. Rott[53, 56], T. Ruhe[23], L. Ruohan[27], D. Ryckbosch[29], I. Safa[14, 40], J. Saffer[32], D. Salazar-Gallegos[24], P. Sampathkumar[31], S. E. Sanchez Herrera[24], A. Sandrock[62], M. Santander[58], S. Sarkar[25], S. Sarkar[47], J. Savelberg[1], P. Savina[40], M. Schaufel[1], H. Schieler[31], S. Schindler[26], L. Schlickmann[1], B. Schlüter[43], F. Schlüter[12], N. Schmeisser[62], T. Schmidt[19], J. Schneider[26], F. G. Schröder[31, 44], L. Schumacher[26], G. Schwefer[1], S. Sclafani[19], D. Seckel[44], M. Seikh[36], S. Seunarine[51], R. Shah[49], A. Sharma[61], S. Shefali[32], N. Shimizu[16], M. Silva[40], B. Skrzypek[14], B. Smithers[4], R. Snihur[40], J. Soedingrekso[23], A. Søgaard[22], D. Soldin[32], P. Soldin[1], G. Sommani[11], C. Spannfellner[27], G. M. Spiczak[51], C. Spiering[63], M. Stamatikos[21], T. Stanev[44], T. Stezelberger[9], T. Stürwald[62], T. Stuttard[22], G. W. Sullivan[19], I. Taboada[6], S. Ter-Antonyan[7], M. Thiesmeyer[1], W. G. Thompson[14], J. Thwaites[40], S. Tilav[44], K. Tollefson[24], C. Tönnis[56], S. Toscano[12], D. Tosi[40], A. Trettin[63], C. F. Tung[6], R. Turcotte[31], J. P. Twagirayezu[24], B. Ty[40], M. A. Unland Elorrieta[43], A. K. Upadhyay[40, 64], K. Upshaw[7], N. Valtonen-Mattila[61], J. Vandenbroucke[40], N. van Eijndhoven[13], D. Vannerom[15], J. van Santen[63], J. Vara[43], J. Veitch-Michaelis[40], M. Venugopal[31], M. Vereecken[37], S. Verpoest[44], D. Veske[46], A. Vijai[19], C. Walck[54], C. Weaver[24], P. Weigel[15], A. Weindl[31], J. Weldert[60], C. Wendt[40], J. Werthebach[23], M. Weyrauch[31], N. Whitehorn[24], C. H. Wiebusch[1], N. Willey[24], D. R. Williams[58], L. Witthaus[23], A. Wolf[1], M. Wolf[27], G. Wrede[26], X. W. Xu[7], J. P. Yanez[25], E. Yildizci[40], S. Yoshida[16], R. Young[36], F. Yu[14], S. Yu[24], T. Yuan[40], Z. Zhang[55], P. Zhelnin[14], M. Zimmerman[40]

[1] III. Physikalisches Institut, RWTH Aachen University, D-52056 Aachen, Germany
[2] Department of Physics, University of Adelaide, Adelaide, 5005, Australia
[3] Dept. of Physics and Astronomy, University of Alaska Anchorage, 3211 Providence Dr., Anchorage, AK 99508, USA
[4] Dept. of Physics, University of Texas at Arlington, 502 Yates St., Science Hall Rm 108, Box 19059, Arlington, TX 76019, USA
[5] CTSPS, Clark-Atlanta University, Atlanta, GA 30314, USA
[6] School of Physics and Center for Relativistic Astrophysics, Georgia Institute of Technology, Atlanta, GA 30332, USA
[7] Dept. of Physics, Southern University, Baton Rouge, LA 70813, USA
[8] Dept. of Physics, University of California, Berkeley, CA 94720, USA
[9] Lawrence Berkeley National Laboratory, Berkeley, CA 94720, USA
[10] Institut für Physik, Humboldt-Universität zu Berlin, D-12489 Berlin, Germany
[11] Fakultät für Physik & Astronomie, Ruhr-Universität Bochum, D-44780 Bochum, Germany
[12] Université Libre de Bruxelles, Science Faculty CP230, B-1050 Brussels, Belgium

PoS(ICRC2023)993

[13] Vrije Universiteit Brussel (VUB), Dienst ELEM, B-1050 Brussels, Belgium
[14] Department of Physics and Laboratory for Particle Physics and Cosmology, Harvard University, Cambridge, MA 02138, USA
[15] Dept. of Physics, Massachusetts Institute of Technology, Cambridge, MA 02139, USA
[16] Dept. of Physics and The International Center for Hadron Astrophysics, Chiba University, Chiba 263-8522, Japan
[17] Department of Physics, Loyola University Chicago, Chicago, IL 60660, USA
[18] Dept. of Physics and Astronomy, University of Canterbury, Private Bag 4800, Christchurch, New Zealand
[19] Dept. of Physics, University of Maryland, College Park, MD 20742, USA
[20] Dept. of Astronomy, Ohio State University, Columbus, OH 43210, USA
[21] Dept. of Physics and Center for Cosmology and Astro-Particle Physics, Ohio State University, Columbus, OH 43210, USA
[22] Niels Bohr Institute, University of Copenhagen, DK-2100 Copenhagen, Denmark
[23] Dept. of Physics, TU Dortmund University, D-44221 Dortmund, Germany
[24] Dept. of Physics and Astronomy, Michigan State University, East Lansing, MI 48824, USA
[25] Dept. of Physics, University of Alberta, Edmonton, Alberta, Canada T6G 2E1
[26] Erlangen Centre for Astroparticle Physics, Friedrich-Alexander-Universität Erlangen-Nürnberg, D-91058 Erlangen, Germany
[27] Technical University of Munich, TUM School of Natural Sciences, Department of Physics, D-85748 Garching bei München, Germany
[28] Département de physique nucléaire et corpusculaire, Université de Genève, CH-1211 Genève, Switzerland
[29] Dept. of Physics and Astronomy, University of Gent, B-9000 Gent, Belgium
[30] Dept. of Physics and Astronomy, University of California, Irvine, CA 92697, USA
[31] Karlsruhe Institute of Technology, Institute for Astroparticle Physics, D-76021 Karlsruhe, Germany
[32] Karlsruhe Institute of Technology, Institute of Experimental Particle Physics, D-76021 Karlsruhe, Germany
[33] Dept. of Physics, Engineering Physics, and Astronomy, Queen's University, Kingston, ON K7L 3N6, Canada
[34] Department of Physics & Astronomy, University of Nevada, Las Vegas, NV, 89154, USA
[35] Nevada Center for Astrophysics, University of Nevada, Las Vegas, NV 89154, USA
[36] Dept. of Physics and Astronomy, University of Kansas, Lawrence, KS 66045, USA
[37] Centre for Cosmology, Particle Physics and Phenomenology - CP3, Université catholique de Louvain, Louvain-la-Neuve, Belgium
[38] Department of Physics, Mercer University, Macon, GA 31207-0001, USA
[39] Dept. of Astronomy, University of Wisconsin–Madison, Madison, WI 53706, USA
[40] Dept. of Physics and Wisconsin IceCube Particle Astrophysics Center, University of Wisconsin–Madison, Madison, WI 53706, USA
[41] Institute of Physics, University of Mainz, Staudinger Weg 7, D-55099 Mainz, Germany
[42] Department of Physics, Marquette University, Milwaukee, WI, 53201, USA
[43] Institut für Kernphysik, Westfälische Wilhelms-Universität Münster, D-48149 Münster, Germany
[44] Bartol Research Institute and Dept. of Physics and Astronomy, University of Delaware, Newark, DE 19716, USA
[45] Dept. of Physics, Yale University, New Haven, CT 06520, USA
[46] Columbia Astrophysics and Nevis Laboratories, Columbia University, New York, NY 10027, USA
[47] Dept. of Physics, University of Oxford, Parks Road, Oxford OX1 3PU, United Kingdom
[48] Dipartimento di Fisica e Astronomia Galileo Galilei, Università Degli Studi di Padova, 35122 Padova PD, Italy
[49] Dept. of Physics, Drexel University, 3141 Chestnut Street, Philadelphia, PA 19104, USA
[50] Physics Department, South Dakota School of Mines and Technology, Rapid City, SD 57701, USA
[51] Dept. of Physics, University of Wisconsin, River Falls, WI 54022, USA
[52] Dept. of Physics and Astronomy, University of Rochester, Rochester, NY 14627, USA
[53] Department of Physics and Astronomy, University of Utah, Salt Lake City, UT 84112, USA
[54] Oskar Klein Centre and Dept. of Physics, Stockholm University, SE-10691 Stockholm, Sweden
[55] Dept. of Physics and Astronomy, Stony Brook University, Stony Brook, NY 11794-3800, USA
[56] Dept. of Physics, Sungkyunkwan University, Suwon 16419, Korea
[57] Institute of Physics, Academia Sinica, Taipei, 11529, Taiwan
[58] Dept. of Physics and Astronomy, University of Alabama, Tuscaloosa, AL 35487, USA
[59] Dept. of Astronomy and Astrophysics, Pennsylvania State University, University Park, PA 16802, USA
[60] Dept. of Physics, Pennsylvania State University, University Park, PA 16802, USA
[61] Dept. of Physics and Astronomy, Uppsala University, Box 516, S-75120 Uppsala, Sweden
[62] Dept. of Physics, University of Wuppertal, D-42119 Wuppertal, Germany
[63] Deutsches Elektronen-Synchrotron DESY, Platanenallee 6, 15738 Zeuthen, Germany
[64] Institute of Physics, Sachivalaya Marg, Sainik School Post, Bhubaneswar 751005, India
[65] Department of Space, Earth and Environment, Chalmers University of Technology, 412 96 Gothenburg, Sweden
[66] Earthquake Research Institute, University of Tokyo, Bunkyo, Tokyo 113-0032, Japan

Acknowledgements

The authors gratefully acknowledge the support from the following agencies and institutions: USA – U.S. National Science Foundation-Office of Polar Programs, U.S. National Science Foundation-Physics Division, U.S. National Science Foundation-EPSCoR, Wisconsin Alumni Research Foundation, Center for High Throughput Computing (CHTC) at the University of Wisconsin–Madison, Open Science

PoS(ICRC2023)993

Grid (OSG), Advanced Cyberinfrastructure Coordination Ecosystem: Services & Support (ACCESS), Frontera computing project at the Texas Advanced Computing Center, U.S. Department of Energy-National Energy Research Scientific Computing Center, Particle astrophysics research computing center at the University of Maryland, Institute for Cyber-Enabled Research at Michigan State University, and Astroparticle physics computational facility at Marquette University; Belgium – Funds for Scientific Research (FRS-FNRS and FWO), FWO Odysseus and Big Science programmes, and Belgian Federal Science Policy Office (Belspo); Germany – Bundesministerium für Bildung und Forschung (BMBF), Deutsche Forschungsgemeinschaft (DFG), Helmholtz Alliance for Astroparticle Physics (HAP), Initiative and Networking Fund of the Helmholtz Association, Deutsches Elektronen Synchrotron (DESY), and High Performance Computing cluster of the RWTH Aachen; Sweden – Swedish Research Council, Swedish Polar Research Secretariat, Swedish National Infrastructure for Computing (SNIC), and Knut and Alice Wallenberg Foundation; European Union – EGI Advanced Computing for research; Australia – Australian Research Council; Canada – Natural Sciences and Engineering Research Council of Canada, Calcul Québec, Compute Ontario, Canada Foundation for Innovation, WestGrid, and Compute Canada; Denmark – Villum Fonden, Carlsberg Foundation, and European Commission; New Zealand – Marsden Fund; Japan – Japan Society for Promotion of Science (JSPS) and Institute for Global Prominent Research (IGPR) of Chiba University; Korea – National Research Foundation of Korea (NRF); Switzerland – Swiss National Science Foundation (SNSF); United Kingdom – Department of Physics, University of Oxford.

PoS(ICRC2023)993